FPGA implementation of a highly efficient pulse discrimination trigger algorithm for the JUNO large PMTs readout electronics

F. MARINI[1][2][*]

[1] *Dipartimento di Fisica e Astronomia, Università di Padova - Padova, Italy*
[2] *INFN, Sezione di Padova - Padova, Italy*

received 25 March 2020

Summary. — The Jiangmen Underground Neutrino Observatory (JUNO) is a neutrino physics experiment located in China. A 20 kton multipurpose underground Liquid Scintillator (LS) will allow the determination of the neutrino mass hierarchy by measuring the nuclear antineutrino energy spectrum. An excellent energy resolution and a large detector fiducial volume are key ingredients for addressing many important topics in neutrino and astroparticle physics. The LS detector is instrumented by 18000 20 inches PhotoMultiplier Tubes (PMT) which corresponds to about 75% of coverage. The Front-End readout electronics focuses on the Global Control Unit (GCU) board which, thanks to the on-board Field Programmable Gate Array (FPGA), is able to do an online processing of the PMTs waveform, providing first-level trigger requests as well as timing synchronization and data forwarding to the Data Acquisition (DAQ) system. The JUNO experiment requires an evaluation of single photoelectron signals originated by the PMTs and, in this conditions, the signal amplitude is comparable to the electronics background noise. Therefore, the paper aims to describe a new kind of trigger algorithm, featuring a high discrimination power. After having defined its architecture, the test section compares the pulse detection efficiency in low Signal-to-Noise Ratio (SNR) scenarios, with a simple leading-edge trigger.

1. – Introduction

Precise measurements of the θ_{13} neutrino oscillation parameter by the Daya Bay [1], Reno [2] and Double Chooz [3] experiments have opened the path to the determination of the neutrino mass hierarchy. The question whether the ν_3 neutrino mass eigenstate is heavier or lighter than the ν_1 and ν_2 mass eigenstates is one of the remaining undetermined fundamental aspects of the Standard Model in the lepton sector. A medium

---

[*] E-mail: filippo.marini@pd.infn.it

1

baseline reactor neutrino experiment would be able to give an answer to this question without dealing with additional complications arising from neutrinos matter effects [4].

The Jiangmen Underground Neutrino Observatory (JUNO) [5] exploits this approach, featuring 20 kton of Liquid Scintillator (LS) detector and an unprecedent energy resolution target of 3% at 1 MeV. Thanks to the large statistics, JUNO will not only be able to determine the neutrino mass hierarchy but it would also be able to precisely measure the neutrino mixing parameters, θ_{12}, Δm_{12}^2 and Δm_{ee}^2 below the 1% level.

The experiment will detect reactor antineutrinos thanks to the inverse beta decay reaction $\bar{\nu}_e + p \rightarrow e^+ + n$. While the positron will promptly annihilate with an electron, the neutron will undergo a delayed proton capture, defining the signature of the reaction.

The JUNO detector structure is quite simple but impressive [6]: the LS is contained inside a large acrylic sphere (34.5 m diameter), kept in position by a stainless stell truss. This supporting structure holds the inner vessel and almost 20000 large (20 inch) PMTs and about 25000 small (3 inch) PMTs. The described central detector will be placed inside an instrumented water pool that will act both as a Cherenkov muon veto and as a shield against environmental radiation (gammas and neutrinos) coming from the rock. Finally, a top tracker made with the plastic scintillator detectors of the former OPERA experiment at Gran Sasso will be placed on top of the water pool.

2. – The JUNO readout electronics

To comply with the energy resolution requirement, the JUNO readout electronics [7] is designed to follow several guidelines. First of all, the Front-End electronics should be placed very close to the PMTs. This will allow to reach the best performaces in terms of signal-to-noise ratio, preventing the analogue stream from deteriorating over very long cables. To minimize the data readout throughput, the Front-End will not only digitize the data, but it will also perform complex online signal processing and storage, generating trigger primitives and passing on to the DAQ only interesting windows of data. Unfortunately, this design comes with a price: the Front-End electronics must be placed underwater, with the impossibility of replacement or repair. Therefore, high reliability constraints must be followed, as well as power consuption restrictions.

After the Front-End, the rest of the electronics chain will be "dry" (*i.e.*, not underwater and accessible) and will consist of several Back-End Cards (BEC), the Central Trigger Unit (CTU) and the DAQ (fig. 1).

The role of the BEC is to handle all the communications between the Front-End, the CTU and the DAQ; in particular the primitives trigger requests from the "wet" electronics are sent to the CTU, which replies with the timestamp of the global trigger decision. The timestamp is then sent to the Front-End in order to extract the relevant
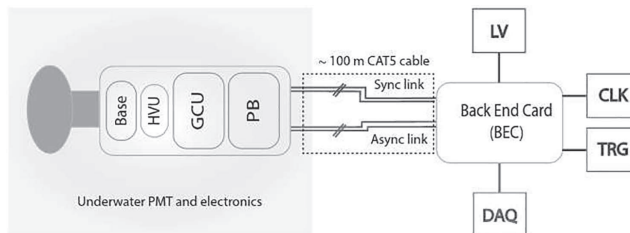

Fig. 1. – JUNO electronics architecture overview.

data window to be sent to the DAQ. The communication between the "wet" and "dry" electronics relies on standard CAT5E cables, with length up to about 100 meters.

2˙1. *Front-End electronics*. – As previously stated, the Front-End electronics is coupled to the PMTs and consists of several components.

- Base: the PMT voltage divider and splitter.

- High Voltage Unit (HVU): a programmable module which provides the bias voltage to the voltage divider.

- Global Control Unit: the intelligent part of the electronics which digitizes the analog signal and performs a first online analysis.

- Power and Communication Board (PB) which provides the inferface to the "dry" electronics driving the synchronous clock and trigger links and providing power to the Front-End.

The CAT5E cable used for communication with the Back-End electronics features four twisted pairs which accommodate:

- an asynchronous link using the 100BASE-TX fast ethernet communication standard;

- a 250 Mbps synchronous link, synchronized with the JUNO clock, Time Division Multiplexed (TDM) to fit both synchronous messages and a digital trigger channel. The protocol foresees the use of Hamming code for 1-bit error correction capability.

A realization of the prototype boards assembled in a castle-like configuration coupled to the PMT is shown in fig. 2.

Figure 3 shows a top (fig. 3(a)) and bottom (fig. 3(b)) photograph of one of the GCU prototypes, the core of the JUNO readout electronics. Its main task consists in the acquisition of the PMT waveform, their processing (local trigger generation, charge reconstruction and timestamp tagging) and temporary storage before sending it to the DAQ upon a trigger request. All these jobs are managed by the FPGA on-board, a
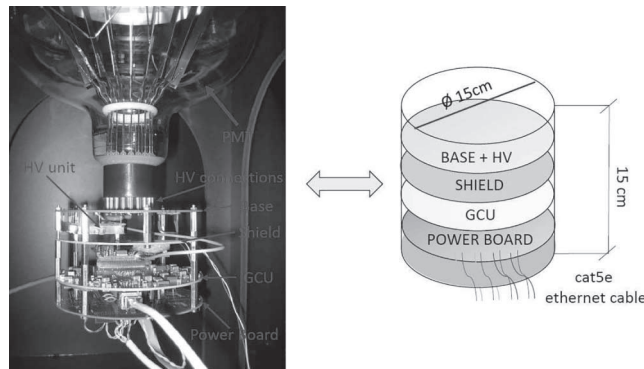

Fig. 2. – The JUNO Front-End readout electronics. The shield component, a blank Printed Circuit Board (PCB), protects the GCU from ElectroMagnetic Interference (EMI) generated by the HVU.

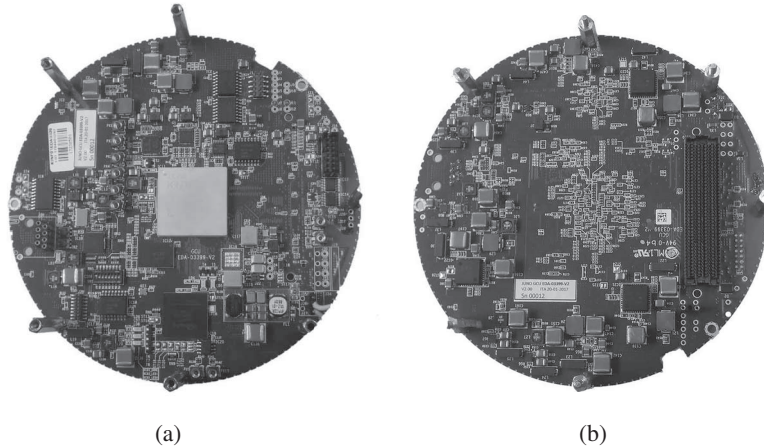(a)   (b)

Fig. 3. – GCU top side (a), and bottom side (b).

Xilinx Kintex-7 (XC7K160T), which is a good compromise between the number of available I/O ports, power consumption, performace and cost. A continuos stream of 14-bit data, sampled at 1 Gsps is transferred from the ADC to the FPGA via 14 LVDS lines (500 MHz DDR). The FPGA is able to handle all the data packaging, processing and buffering.

Upon trigger requests, validated waveforms are sent to the DAQ event builder via Fast Ethernet. The IPBus Core protocol is used for data transfer, slow control monitoring and control operations. The synchronization and communication protocol, running on the synchronous link, is based on the Timing, Trigger and Control (TTC) protocol, developed at CERN. It provides the capability to exchange data between the GCU and the BEC, such as trigger timestamps and calibration information, as well as that of sending trigger inputs upstream to the CTP. The data streams are DC-balanced and the master clock of the experiment is recovered via a Clock and Data Recovery (CDR) chip in the GCU. The synchronization is a key feature: it guarantees that all the 20000 local clocks are aligned with the global time within a system clock period of 16 ns [8].

3. – Pulse-shape processing for trigger requests

In order to improve the single photoelectron (pe) detection and trigger efficiency, a method based on pulse-shape elaboration [9] has been adapted and designed for the JUNO GCU board. The technique is often used for X-ray or germanium detectors signals to retrieve the energy from the signal pulses and reduce the measurements dead time.

Figure 4 shows the structure of the pulse-shape processing, which consists of a 4-module pipeline. The first step dynamically tracks the signal baseline (*i.e.*, the average value of the input signal in the absence of pulses), and is called "baseline follower". The waveform will be further elaborated by the the "k-σ trigger" module, that performs a first signal detection in order to stop the baseline from being evaluated when a signal occurs. Afterwards, the data is used as input of the "Moving Window Deconvolution" (MWD) module, which converts the input pulse into a step function whose amplitude is proportional to the pulse's energy. Proceeding in the chain, the "shaping module"
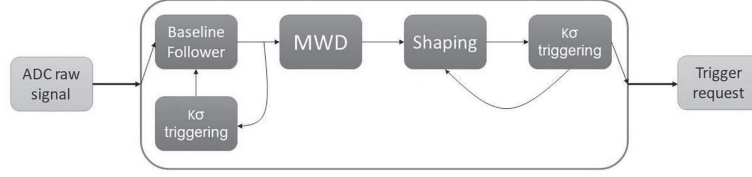
Fig. 4. – Overview of the online, deconvolution-based, pulse-shape analysis.

averages the signal giving it the aspect of a trapezoid or a triangle. This shaped signal is then triggered using a second "k-σ trigger" module.

The algorithm is implemented in the GCUs Kintex 7 FPGA, elaborating the PMTs 14 Gbps digitized data stream coming from the ADU, synchronized to 500 MHz clock in Double Data Rate (DDR) format. Since a 1 GHz clock is not a sustainable frequency for the FPGA, only 1 out of 4 samples are taken into consideration, filtering the stream with a low-pass polyphase decimator filter [10] to avoid aliasing issues.

3'1. *Baseline follower and K-σ trigger*. – The "baseline follower" module has been developed to average out the high frequency amplitude noise and follow the low frequency baseline modulation. The dynamical quantities evaluated for every sampling period are

$$
(1) \qquad B(t_i) = B(t_{i-1}) + \frac{1}{\tau_b}[R(t_i) - B(t_{i-1})],
$$

$$
(2) \qquad \sigma(t_i) = \sigma(t_{i-1}) + \frac{1}{\tau_\sigma}[D(t_i) - \sigma(t_{i-1})],
$$

where t_i is the discrete sampling time, $R(t_i)$ is the raw signal, $B(t_i)$ the baseline, $\sigma(t_i)$ the standard deviation of the noise and $D(t_i)$ the absolute value of the deviation from the baseline of the raw signal, *i.e.*, $D(t_i) = |R(t_i) - B(t_i)|$. τ_b and τ_σ are time constants, expressed in nano-seconds, that reflect the dynamics of the evaluated quantities.

To correctly evaluate the baseline of the raw stream, any pulse must be recognized to freeze the baseline value and resume its evaluation when the pulse returns to the zero value. This job is carried out by the "k-σ trigger" module which dynamically evaluates the deviation od $D(t_i)$ from the baseline in units of $\sigma(t_i)$ to recognize a pulse.

3'2. *Moving Window Deconvolution*. – One of the main advantages of the adopted trigger scheme is to be able to discriminate noise spikes from real signals, even in the case where both of them are beyond the same threshold. The Moving Window Deconvolution (MWD) algorithm [11] is used to exploit the characteristic fast rising edge and an exponential-like decay of the PMT signal to improve the detection efficiency.

From an exponential decay signal, starting at the time $t_0 = 0$, we can model its amplitude at the time t by the expression

$$
(3) \qquad A(t) = \begin{cases} N \exp\left(-\dfrac{t}{\tau}\right) & t \geq 0, \\ 0 & t < 0, \end{cases}
$$

where τ is the decay constant and N the maximum amplitude. We can define a new function $U(t_k)$, with $t_k > 0$, expressed in terms of the initial amplitude N as

$$U(t_k) = A(t_k) + N - A(t_k)$$
$$= A(t_k) + N\left(1 - \exp\left(\frac{-t_k}{\tau}\right)\right)$$
$$= A(t_k) + \frac{1}{\tau}\int_0^{t_k} A(t)\mathrm{d}t$$
$$(4) \qquad = A(t_k) + \frac{1}{\tau}\int_{-\infty}^{t_k} A(t)\mathrm{d}t,$$

where the last step expanding the integral from 0 to $-\infty$ is permitted because the amplitude $A(t_k)$ is zero for $t_k < 0$. $U(t_k)$ aims to obtain a Heavyside step function multiplied by the initial amplitude of the pulse N.

Equation (4) is only valid for positive times. We can easily extend it for negative times giving it the form

$$(5) \qquad U(t) = \begin{cases} N & t \geq 0, \\ 0 & t < 0. \end{cases}$$

With the goal of implementing this algorithm inside an FPGA, we can transform the expression in eq. (4) to the digital domain, retrieving the value N at time t_k,

$$(6) \qquad U(t_k) = A(t_k) + \frac{1}{\tau_d}\sum_{i=-\infty}^{k-1} A(t_i),$$

where $\tau_d = \tau/\Delta t$ is now expressed in units of the sampling time.

Adapting this equation to our signal we obtain

$$(7) \qquad U(t_k) = x(t_k) + \frac{1}{\tau_d}\sum_{i=-\infty}^{k-1} x(t_i),$$

where $x(t_k) = B(t_k) - R(t_k)$. The MWD filter is derived from differentiating the expression in eq. (7),

$$MWD(t_k) = U(t_k) - U(t_{k-w})$$
$$(8) \qquad = x(t_k) - x(t_{k-w}) + \frac{1}{\tau_d}\sum_{i=k-w}^{k-1} x(t_i),$$

where w represents the width of the moving window, as well as the length of the resulting plateau. In order to apply this to a PMT pulse, the first step must consist in estimating the time constant of the exponential decay: τ. If overestimated, the step function will not present a flat top, but a positive slope instead. On the other hand, if underestimated, the flat top is replaced by a negative slope. Since the step function amplitude is correlated to the pulse's energy, a wrong estimation of τ results in a wrong estimation of the energy.

3˙3. *Shaping module*. – The goal of the "shaping module" is to average the plateau provided by the MWD to obtain a unique and well-defined value. This shaping is carried out by a simple Moving Window Average (MWA) filter. As the name suggests, the filter operates by averaging a fixed number of points from the input signal to produce one point in the output signal. This procedure is expressed by the following equation:

$$(9) \qquad MWA(t_k) = \frac{1}{l} \sum_{j=1}^{l} MWD(t_{k-j})$$

where $x(t_k)$, $x(t_{k-1}) \ldots x(t_{k-l})$ are the signal at the discrete sampled times t_k, $t_{k-1} \ldots t_{k-l}$, $MWA(t_k)$ is the output signal at time t_k, and l is the width of the filter window, equal to the number of points in the average. Despite its simplicity, the MWA filter is optimal for a common task: reducing random noise while retaining a sharp step response.

For an easier FPGA implementation, eq. (9) can be rewritten as

$$(10) \qquad MWA(t_k) = MWA(t_{k-1}) + \frac{1}{l}(MWD(t_k) - MWD(t_{k-l-1})).$$

Through this module, the user has the possibility to select between two different shapes. If l is less than w the output will be shaped as a trapezoid, with a $w - l$ long flap top. Instead, if $l = w$, the shape will be the one of a triangle. The advantage of using a trapezoidal form is a greater discriminatory power because of its characteristic plateau; however, if a triangular shape is chosen, the module filtering efficiency will be maximum.

Once the module has shaped the deconvolved output, the standard deviation of the noise's high frequency component is evaluated (eq. (2)) in order to use a "k-σ trigger" to provide the final trigger of the algorithm.

An application of the algorithm to a Hamamatsu R12860-HQE PMT pulse is visible in fig. 5.
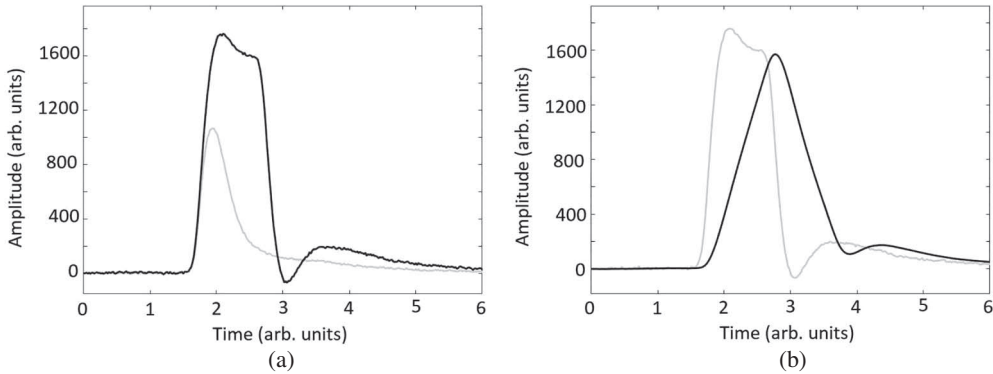

Fig. 5. – (a) MWD module output (black line) resulting from the (inverted) PMT pulse (grey line). (b) Triangular shape output (black line) generated by the shaping module, using a step function (grey line) as input.

4. – Test and results

The proposed trigger algorithm has been tested and characterized to verify its behaviour and performances once implemented in FPGA. In particular the tests aim to:

- verify the correlation relationship between the pulse's energy and the correspondant algorithm output's amplitude;

- compare the low-amplitude pulse discrimination capability of the deconvolution-based proposed algorithm to a simple leading-edge trigger.

4'1. *Trigger energy dependence*. – To control the input energy, the analog signal has been provided by the CAEN DT5810D Fast Digital Detector Emulator [12]. The pulses are set to have a $0.01\,\mu$s rise time, $0.05\,\mu$s decay time and negative polarity, to best simulate a PMT output. The CAEN emulator let the user have complete control over the pulse's parameters, such as amplitude, frequency and, of course, energy.

Figure 6 illustrates the relationship between the digital amplitude of the moving-window-deconvolved-and-shaped triangular waveform and the analogue input pulse voltage amplitude, featuring a strong linear correlation: $r = 0.9998$. Since, throughout the whole test, the rise time and decay time were fixed, this amplitude is proportional to the pulse's energy.

4'2. *Trigger efficiency*. – The signal source for this test is a 20 inch Hamamatsu R12860-HQE PMT, secured inside a dark box. The signal output has been fed to the GCU, with the FPGA firmware accommodating both a leading edge trigger and the deconvolution-based algorithm. Inside the box, the PMT pulses originate from a Light Emitting Diode (LED), whose power is supplied by a pulser with user-set parameters. The trigger efficiency can be defined as

$$(11) \qquad Trigger\ Efficiency = Valid\ Trigger\ Requests/Total\ Trigger\ Requests,$$
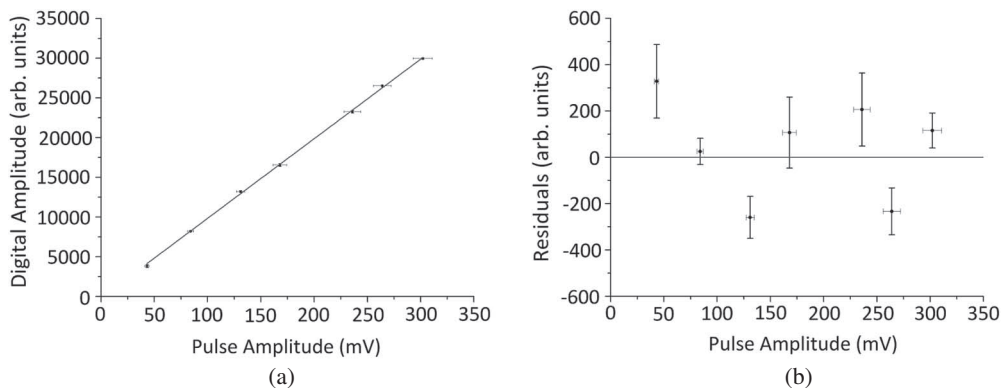

Fig. 6. – (a) Digital amplitudes of the resulting triangular waves as a function of the pulse's voltage amplitude. (b) Residual plot of the triangular waves digital amplitudes reported in fig. 6(a). The arbitrary units used in the two plots are equal.
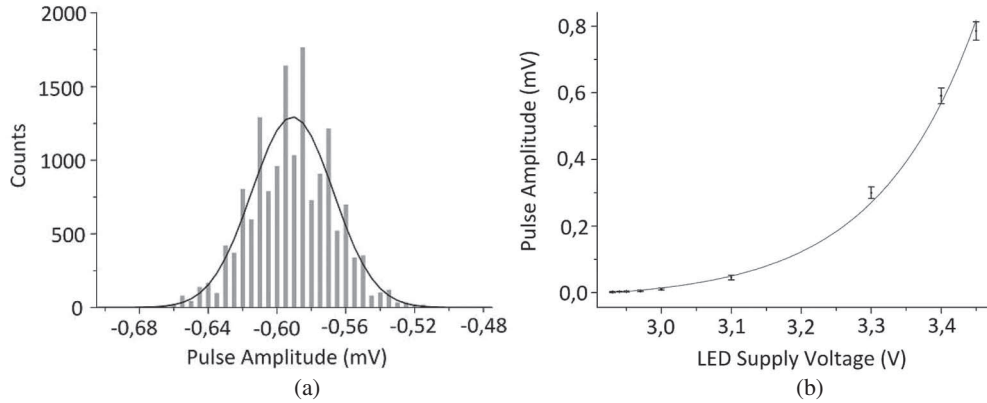
Fig. 7. – (a) Gaussian distribution of the PMT's output pulse amplitude corresponding to a fixed LED supply voltage. (b) Pulse amplitude as a function of the LED supply voltage. The error bars refer to the Gaussian distribution's standard deviation.

where

- *Total trigger requests* are obtained by an unconstrained acquisition of the GCU trigger output. These trigger requests can be generated by the PMT dark noise, residual light penetrating into the dark-box, the LED light and electronics background noise in case of a low threshold level.

- *Valid trigger requests* are the fraction of the *total trigger requests* that overlaps with the LED pulse trigger output, supplied by the LED pulser. *Valid trigger requests* are therefore trigger requests generated only by the LED.

Figure 7 shows the realtionship between the LED supply voltage and the PMT pulse amplitude. An exponential function has been fit through the data points.
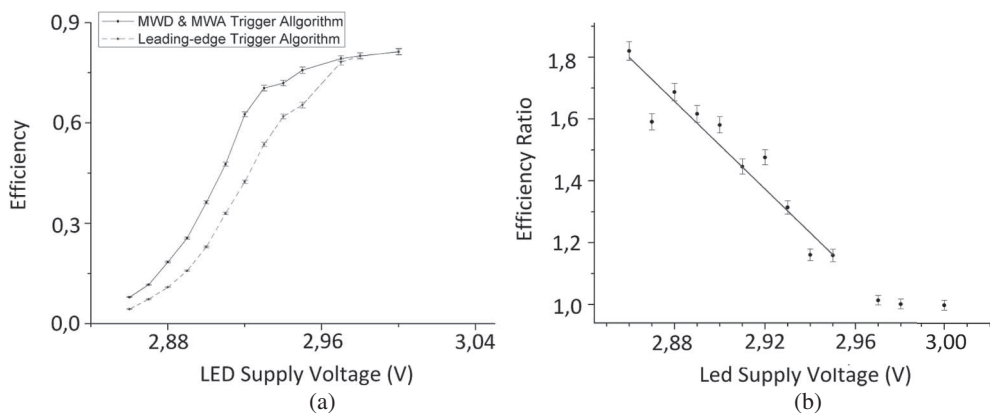

Fig. 8. – (a) Efficiency scan for different LED supply voltages. The solid line refers to the deconvolution-based algorithm, while the dotted line refers to a leading-edge algorithm. (b) Efficiency ratio scan for different LED supply voltages between the two algorithms under test.

TABLE I. – *Dark efficiency results.*

LED supply voltage	MWD-MWA trigger alg.			Leading-edge trigger alg.		
V	Valid trg	Total trg	Efficiency	Valid trg	Total trg	Efficiency
2.86	4	54096	7e−5	18	26214	7e−4

Finally, an efficiency scan is performed at different LED supplied voltages. The results are plotted in fig. 8(a). As expected, the more the LED supply voltage is increased, the easier it is to discriminate the PMT's pulses from the electronic's background noise and the difference in the efficiency becomes negligible. Vice versa, decreasing the LED supply voltage, the pulse's amplitude gets closer to the noise amplitude and the efficiency of the deconvolution-based algorithm in discriminating the real LED-caused PMT pulses is greater compared to the simple leading edge trigger. The efficiency comparison is more clear in fig. 8(b), where the efficiency ratio is plotted. For sufficiently low LED supply voltages, the results manifest a linear relationship with a negative slope. The correlation coefficient is $r = -0.9522$. To make sure that the *valid trigger requests* actually come from LED light, an acquisition on the lowest threshold level is run, keeping the LED off. The results are shown in table I, confirming that the systematic error caused by this sort of *dark efficiency* is compatible with the zero value.

5. – Conclusion

The MWD-MWA trigger algorithm has been successfully implemented in FPGA. The tests performed with a real PMT demonstrate an effective improvement in the discrimination capacity of low-amplitude signals, higlighting an efficiency improvement close to a factor of two when compared to a simple leading-edge trigger. The proposed algorithm could be used by the Front-End readout electronics of the JUNO experiment, increasing the trigger efficiency for the single pe detection, crucial for reaching the target energy resolution.

REFERENCES

[1] DAYA BAY COLLABORATION (AN F. P. *et al.*), *Phys. Rev. Lett.*, **108** (2012) 171803.
[2] RENO COLLABORATION (AHN J. K. *et al.*), *Phys. Rev. Lett.*, **108** (2012) 191802.
[3] DOUBLE CHOOZ COLLABORATION (ABE Y. *et al.*), *Phys. Rev. Lett.*, **108** (2012) 131801.
[4] PETCOV S. T. and PIAI M., *Phys. Lett. B*, **533** (2002) 94.
[5] AN F. P. *et al.*, *J. Phys. G*, **43** (2016) 030401, arXiv:1507.05613.
[6] ADAM T. *et al.*, *JUNO Conceptual Design Report*, arXiv:1508.07166.
[7] BELLATO M. *et al.*, *Embedded Readout Electronics R&D for the Large PMTs in the JUNO Experiment*, arXiv:2003.08339.
[8] PEDRETTI D. *et al.*, *IEEE Trans. Nucl. Sci.*, **66** (2019) 1151, arXiv:1806.04586v2.
[9] STOICA V. IONUT, *Digital pulse-shape analysis and controls for advanced detector systems*, PhD Thesis, Groningen (2012).
[10] ROCCA FABIO, *Elaborazione Numerica dei Segnali* (Edizioni CUSL Milano) 2010.
[11] KAVATSYUK M. *et al.*, *Nucl. Instrum. Methods A*, **648** (2011) 77.
[12] CAEN DT5180, https://www.caen.it/products/dt5810/.